Highlights

- Dynamic and bulk flow properties of powders used in additive manufacturing are characterised using powder rheometry.
- Specimens for mechanical performance measurements are fabricated using selective laser sintering.
- Absolute volume of fabricated sample cubes is determined using helium pycnometry.
- Tensile behaviour and surface hardness of fabricated specimen are correlated to the flowability of powders.

Correlating polyamide powder flowability to mechanical properties of fabricated parts

Reza Baserinia[a,*], Katrina Brockbank[b], Rajeev Dattani[c]

[a]*School of Engineering and Sustainable Development, Faculty of Computing, Engineering and Media, De Montfort University, Leicester, LE1 9BH, United Kingdom*
[b]*Freeman Technology Ltd, 1 Miller Court, Severn Drive, Tewkesbury, Gloucestershire, GL20 8DN, United Kingdom*
[c]*Micromeritics UK, 1 Miller Court, Severn Drive, Tewkesbury, Gloucestershire, GL20 8DN, United Kingdom*

Abstract

This study investigates the relationships between the flow properties of five blends of polyamide 12, with the mechanical and physical characteristics of the fabricated components. The bulk properties and flowability of the powder blends were characterised using powder rheology. Absolute, or skeletal volume of 3D printed cubes were measured using helium pycnometry. The tensile behaviour and surface hardness of specimens fabricated from the five blends were determined. The mechanical properties of the samples were correlated with the flow behaviour of the powder used.

Comparison of the powder flow measures with the mechanical properties of the fabricated parts allows for prediction of final product quality prior to printing. Understanding the relationships between these parameters helps to identify and develop powders that enhance both process efficiency and the mechanical properties of the final product.

Keywords: Additive manufacturing, Powder bed fusion, Selective laser sintering, Powder flow properties, Mechanical performance

*Corresponding author:
Email address: reza.baserinia@dmu.ac.uk

1. Introduction

Selective Laser Sintering (SLS) is an Additive Manufacturing technique used for fabricating complex functional components. SLS can be employed to manufacture parts from metals, polymers, alloy and composite powders [1, 2]. The application has also been extended to the pharmaceutical and food industries [3, 4].

During SLS of polymeric materials, the temperature of the print chamber is initially increased, close to the melting point of the material to reduce the residual stresses during sintering. The process then employs a laser beam to sinter powdered material, binding particles together to create a solid structure. The laser selectively fuses pre-defined areas of a powder bed by scanning cross-sections generated from a 3D digital description of the required part. After each cross-section is scanned, a new layer of material is transferred across from the source using a roller/ blade followed by sintering. This process is repeated until the part is complete. A schematic diagram of the SLS process is presented in Figure 1.

[Figure 1 about here.]

Generating the individual layers of powder is a precision process and requires a feedstock that can be reliably deposited on to the fabrication bed in a consistent manner without agglomerates or voids. This deposition process is governed by flow properties of the powder. Intermittent flow, or agglomerates within the bulk, will cause non-uniform deposition, adversely affecting the efficiency of the process and the properties of the final product. Identifying which flow properties are conducive with the formation of uniform and repeatable layers allows new formulations to be optimised, and suitable raw materials to be identified, without incurring the significant financial and time overheads associated with running materials through the process to assess compatibility. This approach also helps reduce the occurrence of final products that are out of specification.

Different methods have been developed to assess powder flow behaviour under static, dynamic and defined consolidation states [5]. Static methods include

Carr's index [6], Hausner ratio [7], angle of repose [8] and flow factor calculation using shear cell testing [9]. In static methods, the powder initially flows into a static condition before a flow measurement.

In dynamic methods, such as powder rheology [10] and avalanche angle [11, 12], flowability is characterised while the powder is flowing under conditions close to those the powder experiences in the process under investigation. In defined consolidation state methods, the powder is consolidated under external stresses followed by shearing to measure material strength [13]. For the SLS process, since the powder is continuously transferred from supply chamber to the print bed before a small compression is applied by the roller (or the blade), dynamic methods provide flow measures at powder stresses closer to what the material experiences in the real process.

Powder transfer in the SLS process is to some extent similar to linear shoe-die systems used in powder metallurgy and pharmaceuticals whereby the powder is linearly transferred before being deposited into a die (print bed in case of the SLS) while interacting with air in the process. The influence of air-powder interactions in powder delivery processes has been investigated. Baserinia et al. examined the influence of negative air pressure on powder arching [14] and mass flow rate [15] in hopper discharge. Wu et al. [16] examined how the shoe velocity influences the mass of powder discharged into the die. This work was extended by Baserinia and Sinka [17] to investigate air effects in linear feeding systems.

For additive manufacturing applications, Amado et al. [18] used indexes calculated from avalanche angle measurements to characterise powder flowability. Laumer et al. [19] introduced the degree of coverage index as a measure of powder flowability for powder based additive manufacturing applications. Suitability of different powder flow characterisation methods were examined by Clayton et al. [20]. They reported different case studies to examine the influence of batch and manufacturing variations, additives, and powder recycling on powder flowability and proposed powder rheology as a suitable method for powder flow testing in AM applications. Ziegelmeier et al. [21] examined correlation

between the flow behaviour of some polymers to the mechanical performance of fabricates specimens. They observed improved mechanical properties for powders with better flowability. Van den Eynde et al. [22] examined surface defects and packing density of polyamide powders using an apparatus similar to linear shoe-die feeding system and proposed layer density as the index for assessing powder flowability. They extended their study by incorporating a heater into their system to examine flowability at elevated temperatures [23] and observed small increase in the packing density at temperatures above glass transition. The effect of temperature on powder flowability was also investigated by Ruggi et al. [24] through shear cell testing of polyamide 12 (PA12). They observed deterioration of flowability at temperatures close to the melting point of the polymer. In another study, Ruggi et al. [25] showed a significant correlation between the granular Bond number and powder flowability at increased temperatures. Sillani et al. [26] reported an increase in thermal conductivity when packing density of AM powders was increased. Blümel et al. [27] and Schmidt et al. [28] proposed manufacturing processes to produce particles with improved flow properties to achieve tighter packing density and improved part performance in laser beam melting.

Numerical simulation of the powder transfer in SLS additive manufacturing has been carried out using discrete element modelling (DEM) to study powder spreader kinematics [29] as well as jamming [30], segregation [31] and dispersion [32] of particles. However, DEM requires rigorous calibration of input parameters which is a challenging procedure especially for cohesive powders [25].

In this study, two grades of PA12 are mixed to create five custom blends with different ratios of the constituents. Although both grades are of the same material, mixing them can alter the flow behaviour and affect the final properties of the 3D printed part. Hence, the dynamic flow properties of the custom blends are characterised using a FT4 Powder Rheometer® (Freeman Technology Ltd, UK). The flow properties are compared against the absolute volume, tensile behaviour and surface hardness of samples fabricated from these powders to investigate the correlations between powder flowability and mechanical

properties of components. This enables tailoring powders to achieve parts with desired properties without incurring costs associated with trial and testing and over-engineering of particles.

2. Materials

Two commercially available grades of PA12 manufactured by Sinterit, Poland were used in this study. The first grade, PA12 Smooth – Print Ready (PR), contains particles mostly inside the 20 - 100 μm size range with median (d50) of 42 μm based on equivalent circular area diameter (ECAD). The second grade, PA12 Smooth – Fresh (Fresh), has a similar particle size range and the d50 is 37 μm but this grade has smaller shrinking ratio compared to PR (information provided by manufacturer). The particle size distributions of the two grades are shown in Figure 2 which were measured using a Particle Insight Dynamic Image Analyzer manufactured by Particulate Systems, USA. The fine particle contents are dust present in the batches as received from the manufacturer.

[Figure 2 about here.]

Scanning electron microscope (SEM) images of the two grades of PA12 are presented in Figure 3. For each powder, two images at magnifications of 350X and 5000X were captured using an EVO LS 15 microscope (Carl Zeiss, Cambridge, UK.). The samples were gold coated using a Q150RS (Quorum Technologies, Sussex, UK.) prior to imaging.

[Figure 3 about here.]

As is well-known, there is a high proportion of powder from the print bed that is not used in the final part. This powder can be degraded during printing. However, to minimise waste and associated costs, the used powder should ideally be recycled and re-used within the printing process. Of the two materials used here, it is recommended by the manufacturer to mix the recycled PR powder with Fresh grade at a 70:30 ratio to minimise the degradation effect.

However, mixing different grades can potentially alter flowability of the powder and mechanical properties of the final product.

In this study, to evaluate the influence of mixing different grades, five custom blends of PA12 nylon were mixed with different ratios of PR and Fresh (including the ratio recommended by the manufacturer) using virgin powder. The ratios used are summarised in Table 1.

[Table 1 about here.]

3. Methods

3.1. Powder Rheology

Powder rheology measurements were determined using a FT4 Powder Rheometer ® (Freeman Technology Ltd, UK) and the Aeration Control Unit accessory. All measurements were made in triplicate using fresh samples and carried out using the 25 mm internal diameter test vessel and related accessories. Before each measurement, the powder bed was conditioned using the standard conditioning cycle available on the instrument resulting in a consistently packed powder bed.

3.1.1. Dynamic Flow Properties

The flow energy, defined as the resistance of the powder to the blade's motion, was measured using a 23.5 mm twisted blade rotating anti-clockwise at blade tip speed of 100 mm/s passing through 25 ml of sample. The measurements were taken starting at 55 mm and finishing at 5 mm above the powder vessel base following the procedure detailed by Freeman [10]. The FT4 measures axial force (F) and rotational torque (T) as a function of height (H) while the blade traverses downwards through the powder bed. The flow energy was then calculated using Equation 1, where R is the radius of the blade (11.75 mm). The flow energy was measured 7 times using 25 ml of sample under alternating Condition and Test cycles. The Basic Flowability Energy (BFE) is defined as the flow energy for the 7^{th} cycle. Prior to taking these measurements, the

conditioned bulk density (CBD) of the powder was calculated using its initial volume and mass.

$$Flow\ Energy = \sum \left[\left(\frac{T}{R \cdot tan\left(\alpha\right)} + F \right) dH \right] \quad (1)$$

During the SLS process, the powder particles are continuously interacting with the air present in the print chamber while a new layer is deposited. Therefore, it is important to establish how powder flow behaviour is influenced when air is passing through the bed. For this purpose, the same flow energy measurement can be carried out while air is passed through the bed. For the data presented here, a face velocity of 2.5 mm/s was used. The BFE is divided by the flow energy at 2.5 mm/s air velocity to give the aeration ratio at 2.5 mm/s ($AR_{2.5}$). The larger the aeration ratio the more sensitive the powder is to fluidisation.

3.1.2. Bulk Powder Properties

A porous vented piston (external diameter 24 mm) was used to apply up to 15 kPa normal stress on 10 ml of sample, while air was simultaneously passed through a porous mesh base underneath the confined powder bed at a face velocity of 2 mm/s. The excess pressure required in order to maintain a constant flow of air was measured, defined as the pressure drop (PD). A higher PD indicates a lower permeability as there is more resistance to the flow of air through the powder bed. Once the pressure drop across the powder bed is determined, permeability can be determined using Darcy's law.

From the same measurements, the compressibility (CPS) of the powder bed was calculated using the change in height of the powder bed as the vented piston applied increasing normal stress from 1 to 15 kPa. The change in volume was determined and the compressibility was calculated using Equation 2.

$$Compressibility\ \% = \frac{Initial\ Volume - Compressed\ Volume}{Initial\ Volume} \times 100 \quad (2)$$

3.2. Selective Laser Sintering

The specimens utilised in this study were fabricated using a Sinterit Lisa SLS 3D printer manufactured by Sinterit, Poland with print bed size of 150 × 200 × 160 mm. When printing, the layer height was set to 0.125 mm and the laser power ratio was set to 1.0 for all powder grades. The print surface temperature offset was left at 0 °C and the chamber temperature was raised to 180 °C before the printing process. The geometry of the specimens was sketched using CAD and the G-code was generated using the dedicated software of the 3D printer.

3.3. Volume and Density Measurement of 3D Printed Parts

For each powder blend, nine 2 cm-sided cubes were fabricated in a 3×3 array inside the print bed, with cube 1 located in the bottom left corner, and cube 9 in the top right. The cubes were equally spaced horizontally within the high accuracy print volume within the print bed (90×130×130 mm). The density of 3D printed cubes was measured using a gas displacement pycnometer, AccuPyc II 1340 (Micromeritics Instrument Corporation, Norcross, GA, USA) using a 35 cm^3 insert in a 100 cm^3 chamber to reduce the dead volume. The equilibrated gas pressure in the sample chamber and the equilibrium gas pressure after the gas was allowed to expand into an empty second chamber allowing for the absolute or skeletal volume to be calculated. For each cube, this cycle was complete 10 times and the average was determined. The mass of each cube was measured on a precision mass balance and the density was calculated.

3.4. Tensile Testing

The geometry of the specimen for tensile testing was sketched according to the ASTM D 638 – 03 Type IV standard. The geometries were positioned in two rows inside of the print volume of the bed with consistent spacing. After fabrication, the tensile behaviour of each specimen was examined using an Instron 3360 tensile testing machine at room temperature with the displacement rate set at 50 mm/min. Five specimens were tested for each powder blend with tests terminating upon failure of the specimen.

3.5. Hardness Testing

The surface hardness of specimens fabricated from the five blends of PA12 was determined using a ZHR Rockwell Hardness Tester manufactured by Zwick-Roell Ltd., UK. For each powder, a 100×20×6 mm was 3D printed and the HRL hardness was determined 10 times on the top surface following the ASTM D785 – 03 standard.

4. Results and Discussions

4.1. Dynamic Flow Measurements

The dynamic flow measurements and the conditioned bulk density of the five PA12 nylon blends are presented in Table 2.

[Table 2 about here.]

It is observed that CBD increases for blends with larger volume of Fresh present. Additionally, the BFE increases with increasing the volume of Fresh present in the blend. Comparison of the BFE for the PR blend with Fresh shows an increase of 37% in the energy required for the blade to traverse downwards through the powder bed on a fixed helical path.

The influence of air and particle interactions on powder flowability is studied using the $AR_{2.5}$. The results show that by increasing the volume of Fresh in the blend, the sensitivity to fluidisation increases exponentially where the $AR_{2.5}$ measured for the Fresh blend is almost three times larger than the value recorded for PR.

4.2. Bulk Powder Properties

The powder compressibility and the pressure drop across the powder bed under a range of normal stresses were measured for the five blends of PA12. The results determined at the maximum normal stress of 15 kPa are summarised in Figure 4 as an example. All measured data are available under the Appendix section.

[Figure 4 about here.]

By increasing the applied normal stress, the PD and CPS percentage increase for all powders the extent of which depends on the volume of Fresh in the blend (Figures A.1 and A.2). The largest increase was observed for PR and PR70 blends where PD and CPS increased by 15% and 4.5% respectively while these increases were limited to 5% and 2% for the Fresh blend.

4.3. Discussion on dynamic flow measurements and bulk powder properties

Cohesive, and poor flowing powders commonly require higher energy for the blade to traverse downward and they exhibit higher compressibility under normal stress due to the presence of voids within their bed structure which also increases the ability of air to pass through the bed [33, 34].

However, this is not always the case and the BFE measured for efficiently packed powder beds (indicative of good powder flowability) can be high since there is less space for particles to rearrange and more force and torque would be needed for the blade to pass through the bed. Therefore, the dynamic flow measurements and bulk powder properties must be interpreted together.

According to the SEM images in Figures 3-a and 3-c, the overall shape and surface features of the two blends are similar. However, closer inspection of the images obtained from individual particles (Figure 3-b and 3-d) shows a large number of nano-sized features on the surface of the PR particles compared to the Fresh. These nano-scale features result in higher particle interlocking in PR grade.

Since all blends are from the same material (same particle density), larger bulk density is correlated to tighter packing of the particles. For powders with larger volume of Fresh the packing density before the application of external normal pressure is higher (evidenced by CBD measurements in Table 2) which reduces the ability of the particles to rearrange when subject to external loads. This results in smaller percentage of compressibility and higher pressure drop (due to smaller blend porosity) as shown in Figure 4. In addition, higher BFE

is measured for these blends showing larger force/torque required for the blade to traverse downward due to lower porosity in the powder bed (Table 2). The results indicate that the addition of Fresh powder results in a denser packed bed and a more free flowing powder.The higher pressure drop and $AR_{2.5}$ also show that as more Fresh grade is added, the blend is readily fluidised and is more sensitive to aeration.

On the other hand, when PR is the dominant grade in the blend, the increased particle interlocking resulted from the surface features lead to smaller initial packing density when the container is filled and increased ability of the particles to rearrange when normal pressure is applied (higher porosity). Therefore, the pressure drop across these blends is smaller and the compressibility percentage is larger. Powders with higher proportion of Fresh are then ranked as better flowing compared to those with PR as the main constituent.

4.4. Volume and Density measurements

The average volume and average density of the nine samples 3D printed from each blend of PA12 are presented in Figure 5. Generally, there are very small variations in the volume measurements (<1% RSD) taken from the specimens of similar blend showing consistent distribution of the powder across the print bed prior to fabrication. On the other hand, comparing average sample volume of different blends shows that the values measured for specimens made from blends with higher levels of Fresh are much larger than the target volume of 8 cm^3 indicating poorer geometrical tolerance. For example, the average volume of the samples fabricated from PR30 is 13% larger than the average volume determined for PR70. Poor dimensional accuracy is a known issue in SLS manufacturing [35]. Tighter particle packing results in increased conductive heat transfer to surrounding particles during laser sintering [26] and the particles that are further away from the laser path are sintered to those in close proximity of it which adversely influences the geometrical accuracy of the fabricated samples. The smaller shrinking ratio of the Fresh grade is another factor affecting the final size of the samples. The difference in the average volumes is not translated into

average densities due to the difference in shrinking ratio of PR and Fresh grades and the values obtained are close to each other. Therefore, although the bulk density of the powders prior to fabrication is different, the final parts are of similar density.

[Figure 5 about here.]

4.5. Tensile Behaviour of 3D Printed Samples

The width and thickness of the narrow section of the tensile testing specimens were measured in the middle and within 5 mm of each end of the gauge length. The average values calculated for each powder are summarised in Figure A.3 for reference. Comparison of the results shows similar observations to volume measurement specimens in terms of the geometrical accuracy; and the width and thickness values are shown to be on average 5.6% and 8.1% larger than the target sizes of 6.0 and 3.2 mm respectively (target sizes based on ASTM D 638 – 03 Type IV standard). Each specimen was then subjected to a tensile force following the procedure explained in Section 3.4. The force - displacement curve obtained for a PR50 specimen is shown in Figure A.4 as an example. Initially, the specimens undergo elastic deformation with the force increasing linearly with the displacement followed by a plateauing increase of force indicating plastic deformation. Sample breakage resulted in a sudden drop in the force and termination of the testing.

The force - displacement measurements were used to determine the changes in the tensile stress and strain summarised in Figures 6 and 7 respectively. For powders with higher values of BFE and denser bed packing (higher %Fresh), the mechanical performance is improved where the tensile strengths determined were larger both at the peak and at break point; and the samples maintained higher strains before breakage. For example, comparison of the results obtained for the Fresh blend with PR shows a 37% increase in the maximum tensile strength. Similar trends were observed when the Young's modulus of the samples (determined for the linear region of the stress-strain curve) were compared

against each other. In better flowing powders, the improvement in mechanical performance is attributed to stronger bonds between the particles after sintering which have resulted from tighter bed packing. In PR, the surface features on the particles (Figure 3-b) reduce the contact area between the particles especially when the contact is only between the features of adjacent particles. This results in weaker bonds after sintering and reduced mechanical performance. It can therefore be concluded that better powder flowability results in denser particle packing with uniformly distributed pores which then leads to improved performance of the fabricated parts. Consequently, flow characterisation of available blends before fabrication, can provide a predictor for relative mechanical performance.

Comparing the BFE measurements presented in Table 2 with the maximum tensile strengths (Figure 8) shows a linear correlation. Similar material specific charts can be generated to enable estimation of the tensile strength from dynamic flow characteristics of the powder blend before 3D printing.

[Figure 6 about here.]

[Figure 7 about here.]

[Figure 8 about here.]

4.6. Rockwell Hardness of 3D Printed Samples

The average HRL hardness values measured using the specimens fabricated from the five blends of PA12 are presented in Figure 9-a. It is shown that the surface hardness of the samples increases exponentially when the portion of the Fresh in the blend is increased whereby the hardness measured for the sample fabricated from the Fresh grade is approximately four times larger than the hardness determined for those made from PR. This is significantly larger than the improvements in the tensile behaviour of the specimens. Superior surface hardness of the samples with larger portion of Fresh is attributed to improved particle packing and pore distribution resulted from better powder flowability of the blends.

Similar to tensile strength, the relationship between the dynamic flow characteristics (e.g. BFE) and the hardness data can be used to predict the surface hardness of the components prior to fabrications (Figure 9-b).

[Figure 9 about here.]

5. Conclusions

In this study, five custom blends mixed from different ratios of two commercially available grades of PA12 with similar particle size distribution were used to analyse the correlations between powder flow characteristics and the mechanical performance of samples manufactured using the SLS technique. Dynamic flow characterisation and bulk powder properties of the blends showed that for powders with larger portion of Fresh, the BFE and CBD values were higher indicating improved flowability. Poor flow behaviour of powders with bigger portion of PR is associated with the significant number of features on the surface of the PR particles. These features increase particle interlocking and reduce the ability of the particles to flow against each other. Mechanical performance of the samples fabricated from the five blends were analysed using tensile testing and surface hardness measurements. Better flowing powders (higher %Fresh) were shown to have superior mechanical properties, where the tensile strength, tensile strain and the HRL Rockwell hardness determined for the samples made from these blends were greater than the values obtained for other samples. The mechanical properties are determined by the initial state of the powder bed before sintering. Powders with better flowability have tighter particle packing in the print bed and the pores are distributed uniformly which result in stronger bonds between the particles after sintering and in turn improves the mechanical performance of the fabricated component. Despite the mechanical improvements in samples made from better flowing powders, the geometrical accuracy of these parts was shown to be poorer compared to those fabricated from the blends with PR grade as the main constituent. Tighter particle packing increases convective heat transfer between the particles in the sintering zone and the surrounding

particles and greater number of particles bond together increasing the final size of the component. Therefore, in the design stage, the CAD file of the component must be adjusted based on the flowability of the material in use and its packing density. The dynamic and bulk flow characteristics of the powders are shown to be good indicators of the mechanical performance of fabricated components where better flowing powders show superior properties. Charts and diagrams can be generated for materials with multiple grades (different size distributions/ surface features) to relate the flow measures to mechanical properties and use them in the design stage to tailor the powder to required performance. This approach reduces the manufacturing costs through lower waste generation in trial and error and fabrication of samples with insufficient performance. Moreover, it helps to avoid fabricating samples with properties greater than required and unnecessary addition to the manufacturing costs since the grades with better flow properties have undergone sophisticated and controlled manufacturing processes and are therefore more expensive.

CRediT Authorship Contribution Statement

Reza Baserinia: Supervision, Funding acquisition, Project administration, Investigation, Formal analysis, Writing - Original Draft. **Katrina Brockbank:** Investigation. **Rajeev Dattani:** Supervision, Project administration, Formal analysis, Writing - Review & Editing.

Acknowledgements

This work was partially supported by De Montfort University, Leicester, United Kingdom.

Declaration of Competing Interest

None.

References

[1] T. D. Ngo, A. Kashani, G. Imbalzano, K. T. Q. Nguyen, D. Hui, Additive manufacturing (3d printing): A review of materials, methods, applications and challenges, Composites Part B: Engineering 143 (2018) 172–196, iD: 271637. doi:https://doi.org/10.1016/j.compositesb.2018.02.012.

[2] B. Chen, R. Davies, Y. Liu, N. Yi, D. Qiang, Y. Zhu, O. Ghita, Laser sintering of graphene nanoplatelets encapsulated polyamide powders, Additive Manufacturing 35 (2020) 101363. doi:https://doi.org/10.1016/j.addma.2020.101363.
URL https://www.sciencedirect.com/science/article/pii/S2214860420307351

[3] F. Fina, A. Goyanes, S. Gaisford, A. W. Basit, Selective laser sintering (sls) 3d printing of medicines, International Journal of Pharmaceutics 529 (1) (2017) 285–293, iD: 271189. doi:https://doi.org/10.1016/j.ijpharm.2017.06.082.

[4] J. I. Lipton, M. Cutler, F. Nigl, D. Cohen, H. Lipson, Additive manufacturing for the food industry, Trends in Food Science & Technology 43 (1) (2015) 114–123, iD: 271911. doi:https://doi.org/10.1016/j.tifs.2015.02.004.

[5] D. Barletta, M. Poletto, A. C. Santomaso, Chapter 4 Bulk Powder Flow Characterisation Techniques, Powder Flow: Theory, Characterisation and Application, The Royal Society of Chemistry, 2019, pp. 64–146, jF:; JO:. doi:10.1039/9781788016100-00064.

[6] R. L. Carr, Evaluating flow properties of solids, Chemical Engineering 72 (1965) 247–260.

[7] H. H. Hausner, Friction conditions in a mass of metal powder, International Journal of Powder Metallurgy 3 (4) (1967) 7–13.

[8] D. Geldart, E. C. Abdullah, A. Hassanpour, L. C. Nwoke, I. Wouters, Characterization of powder flowability using measurement of angle of repose, China Particuology 4 (3) (2006) 104–107, iD: 274156. doi:https://doi.org/10.1016/S1672-2515(07)60247-4.

[9] A. W. Jenike, Storage and Flow of Solids, University of Utah, United States, 1964.

[10] R. Freeman, Measuring the flow properties of consolidated, conditioned and aerated powders — a comparative study using a powder rheometer and a rotational shear cell, Powder Technology 174 (1) (2007) 25 – 33, special Edition from the PSA2005 Conference. doi:https://doi.org/10.1016/j.powtec.2006.10.016.

[11] M. A. Carrigy, Experiments on the angles of repose of granular materials 1, Sedimentology 14 (3-4) (1970) 147 – 158.

[12] G. Lumay, F. Boschini, K. Traina, S. Bontempi, J.-C. Remy, R. Cloots, N. Vandewalle, Measuring the flowing properties of powders and grains, Powder Technology 224 (2012) 19 – 27. doi:https://doi.org/10.1016/j.powtec.2012.02.015.

[13] H. Shi, R. Mohanty, S. Chakravarty, R. Cabiscol, M. Morgeneyer, H. Zetzener, J. Y. Ooi, A. Kwade, S. Luding, V. Magnanimo, Effect of particle size and cohesion on powder yielding and flow, KONA Powder and Particle Journal 35 (2018) 226–250. doi:10.14356/kona.2018014.

[14] R. Baserinia, I. C. Sinka, P. Rajniak, Vacuum assisted flow initiation in arching powders, Powder Technology 301 (2016) 493–502. doi:https://doi.org/10.1016/j.powtec.2016.03.051.

[15] R. Baserinia, I. C. Sinka, Mass flow rate of fine and cohesive powders under differential air pressure, Powder Technology 334 (2018) 173–182, iD: 271376. doi:https://doi.org/10.1016/j.powtec.2018.04.041.

[16] C.-Y. Wu, L. Dihoru, A. C. Cocks, The flow of powder into simple and stepped dies, Powder Technology 134 (1) (2003) 24–39. doi:https://doi.org/10.1016/S0032-5910(03)00130-X.

[17] R. Baserinia, I. Sinka, Powder die filling under gravity and suction fill mechanisms, International Journal of Pharmaceutics 563 (2019) 135–155. doi:https://doi.org/10.1016/j.ijpharm.2019.01.068.
URL https://www.sciencedirect.com/science/article/pii/S0378517319301103

[18] A. Amado, M. Schmid, K. Wegener, Flowability of sls powders at elevated temperature, Tech. rep., Zürich (2014). doi:10.3929/ethz-a-010057815.

[19] T. Laumer, T. Stichel, M. Raths, M. Schmidt, Analysis of the influence of different flowability on part characteristics regarding the simultaneous laser beam melting of polymers, Physics Procedia 83 (2016) 937–946, laser Assisted Net Shape Engineering 9 International Conference on Photonic Technologies Proceedings of the LANE 2016 September 19-22, 2016 Fürth, Germany. doi:https://doi.org/10.1016/j.phpro.2016.08.098.
URL https://www.sciencedirect.com/science/article/pii/S187538921630205X

[20] J. Clayton, D. Millington-Smith, B. Armstrong, The application of powder rheology in additive manufacturing, Jom 67 (3) (2015) 544–548.

[21] S. Ziegelmeier, P. Christou, F. Wöllecke, C. Tuck, R. Goodridge, R. Hague, E. Krampe, E. Wintermantel, An experimental study into the effects of bulk and flow behaviour of laser sintering polymer powders on resulting part properties, Journal of Materials Processing Technology 215 (2015) 239 – 250. doi:https://doi.org/10.1016/j.jmatprotec.2014.07.029.

[22] M. Van den Eynde, L. Verbelen, P. Van Puyvelde, Assessing polymer powder flow for the application of laser sintering, Powder Technology 286 (2015) 151 – 155. doi:https://doi.org/10.1016/j.powtec.2015.08.004.

[23] M. Van den Eynde, L. Verbelen, P. Van Puyvelde, Influence of temperature on the flowability of polymer powders in laser sintering, AIP Conference Proceedings 1914 (1) (2017) 190007. doi:10.1063/1.5016796.

[24] D. Ruggi, C. Barrès, J.-Y. Charmeau, R. Fulchiron, D. Barletta, M. Poletto, A quantitative approach to assess high temperature flow properties of a pa 12 powder for laser sintering, Additive Manufacturing 33 (2020) 101143. doi:https://doi.org/10.1016/j.addma.2020.101143.

[25] D. Ruggi, M. Lupo, D. Sofia, C. Barrès, D. Barletta, M. Poletto, Flow properties of polymeric powders for selective laser sintering, Powder Technology 370 (2020) 288 – 297. doi:https://doi.org/10.1016/j.powtec.2020.05.069.

[26] F. Sillani, F. de Gasparo, M. Schmid, K. Wegener, Influence of packing density and fillers on thermal conductivity of polymer powders for additive manufacturing, The International Journal of Advanced Manufacturing Technology (2021) 1–10.

[27] C. Blümel, M. Sachs, T. Laumer, B. Winzer, J. Schmidt, M. Schmidt, W. Peukert, K.-E. Wirth, Increasing flowability and bulk density of pe-hd powders by a dry particle coating process and impact on lbm processes, Rapid Prototyping Journal (2015).

[28] J. Schmidt, M. Sachs, S. Fanselow, M. Zhao, S. Romeis, D. Drummer, K.-E. Wirth, W. Peukert, Optimized polybutylene terephthalate powders for selective laser beam melting, Chemical Engineering Science 156 (2016) 1–10. doi:https://doi.org/10.1016/j.ces.2016.09.009.
URL https://www.sciencedirect.com/science/article/pii/S0009250916304894

[29] S. Haeri, Y. Wang, O. Ghita, J. Sun, Discrete element simulation and experimental study of powder spreading process in additive manufacturing, Powder Technology 306 (2017) 45 – 54. doi:https://doi.org/10.1016/j.powtec.2016.11.002.

[30] W. Nan, M. Pasha, T. Bonakdar, A. Lopez, U. Zafar, S. Nadimi, M. Ghadiri, Jamming during particle spreading in additive manufacturing, Powder Technology 338 (2018) 253 – 262. doi:https://doi.org/10.1016/j.powtec.2018.07.030.

[31] W. Nan, M. Pasha, M. Ghadiri, Numerical simulation of particle flow and segregation during roller spreading process in additive manufacturing, Powder Technology 364 (2020) 811 – 821. doi:https://doi.org/10.1016/j.powtec.2019.12.023.

[32] M. Ahmed, M. Pasha, W. Nan, M. Ghadiri, A simple method for assessing powder spreadability for additive manufacturing, Powder Technology 367 (2020) 671 – 679. doi:https://doi.org/10.1016/j.powtec.2020.04.033.

[33] T.-T. Nguyen, K.-M. Hwang, S.-H. Kim, E.-S. Park, Development of novel bilayer gastroretentive tablets based on hydrophobic polymers, International Journal of Pharmaceutics 574 (2020) 118865. doi:https://doi.org/10.1016/j.ijpharm.2019.118865.
URL https://www.sciencedirect.com/science/article/pii/S037851731930910X

[34] C. Pitchayajittipong, R. Price, J. Shur, J. S. Kaerger, S. Edge, Characterisation and functionality of inhalation anhydrous lactose, International Journal of Pharmaceutics 390 (2) (2010) 134–141. doi:https://doi.org/10.1016/j.ijpharm.2010.01.028.
URL https://www.sciencedirect.com/science/article/pii/S0378517310000621

[35] E. Olakanmi, R. Cochrane, K. Dalgarno, A review on selective laser sintering/melting (sls/slm) of aluminium alloy powders: Processing, microstructure, and properties, Progress in Materials Science 74 (2015) 401–477. doi:https://doi.org/10.1016/j.pmatsci.2015.03.002.

URL https://www.sciencedirect.com/science/article/pii/S0079642515000389

List of Figures

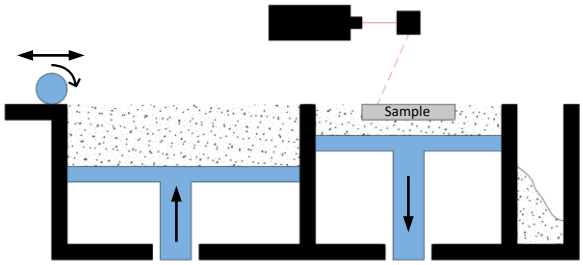

Figure 1: Schematic diagram of Selective Laser Sintering (SLS) process

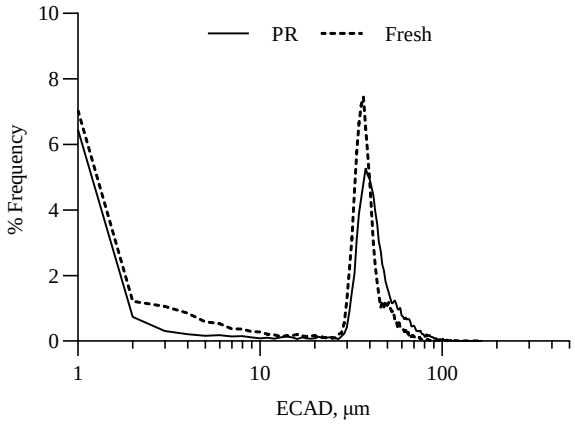

Figure 2: Particle size distribution of PR and Fresh measured using a Particle Insight Dynamic Image Analyzer.

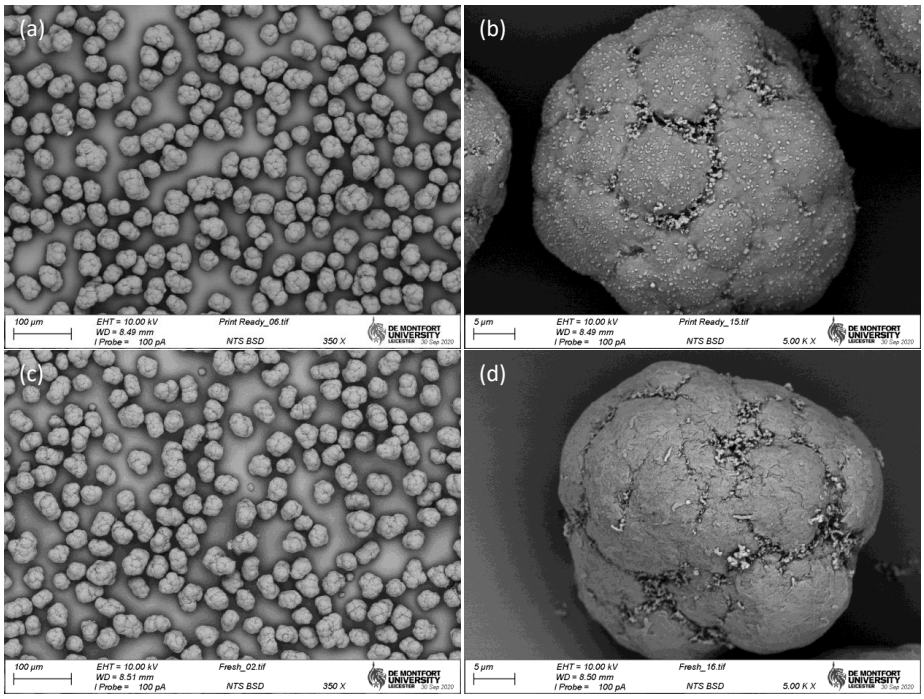

Figure 3: SEM images of PR grade at a) 350X and b) 5000X magnifications and of Fresh grade at c) 350X and d) 5000X magnifications.

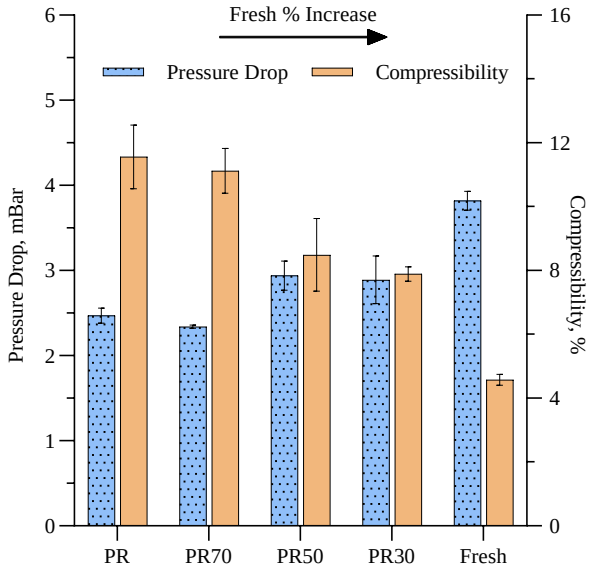

Figure 4: Pressure drop at face velocity of 2 mm/s and compressibility of five blends of PA12 measured at normal pressure of 15 kPa.

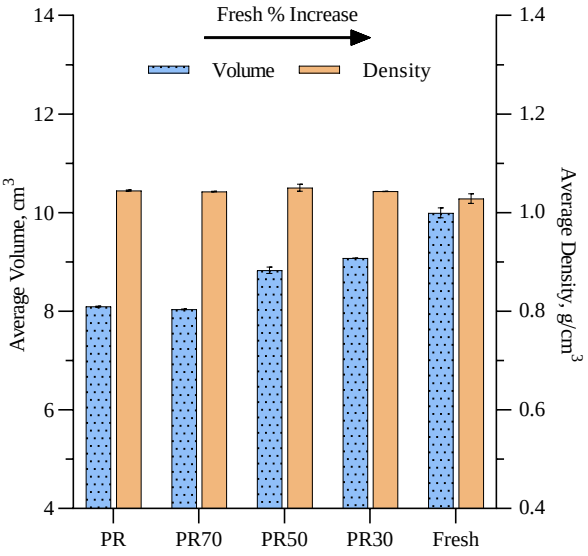

Figure 5: Average volume and density of cubes fabricated from five blends of PA12 measured using helium pycnometry.

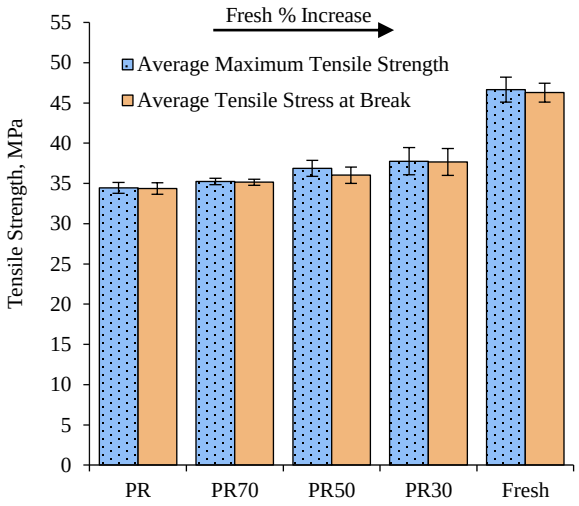

Figure 6: Average maximum tensile strength and average tensile stress at break for for five blends of PA12.

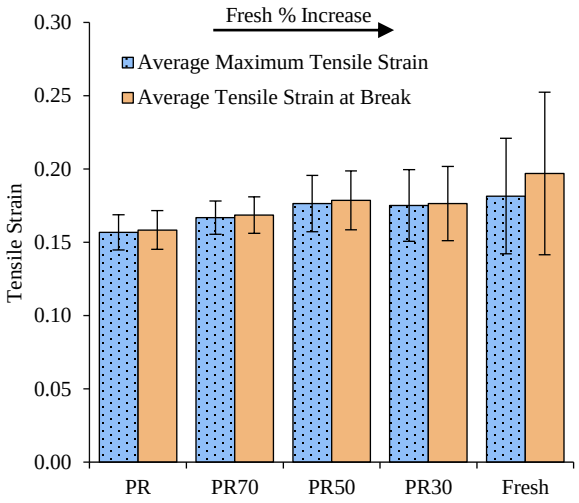

Figure 7: Average maximum tensile strain and average tensile strain at break for for five blends of PA12.

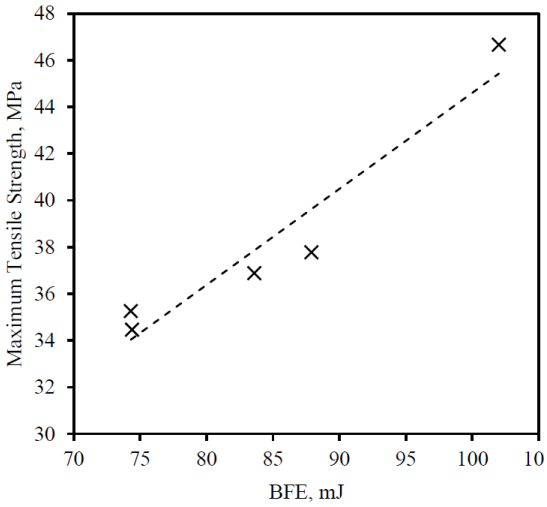

Figure 8: BFE vs. average maximum tensile strength (R^2=0.92) measured for samples fabricated from the five blends of PA12.

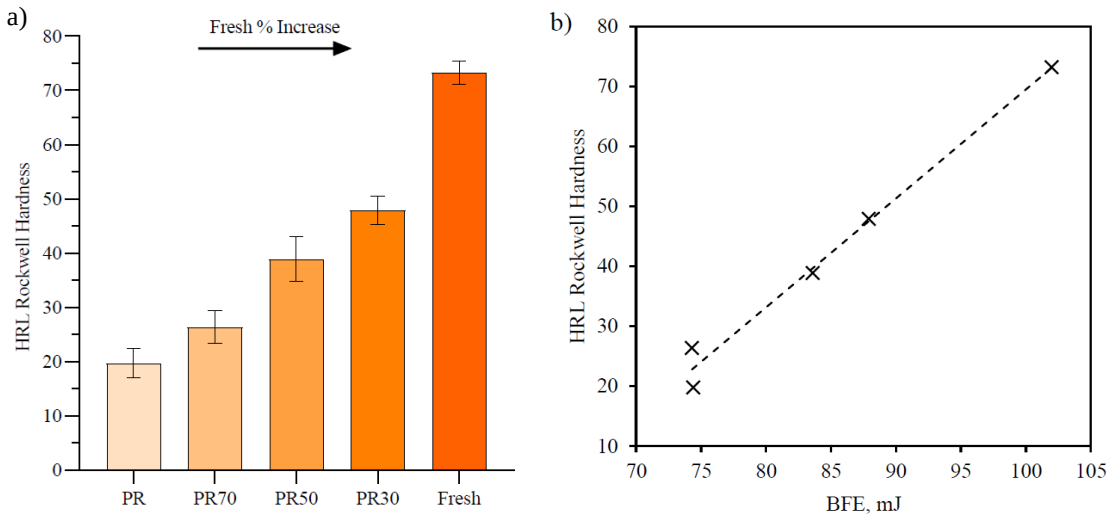

Figure 9: a) Average HRL Rockwell hardness and b) BFE vs. HRL Rockwell hardness (R^2=0.99) measured for samples fabricated from the five blends of PA12.

List of Tables

Table 1: Volumetric ratios of PR and Fresh powders used to mix five blends of PA12.

Powder Blend	Volume % of PR	Volume % of Fresh
PR	100	0
PR70	70	30
PR50	50	50
PR30	30	70
Fresh	0	100

Table 2: Dynamic flow measurements and CBD for five blends of PA12 determined using powder rheometry. The percentage standard deviation between repeat experiments are shown in brackets.

Powder Blend	CBD, g/ml	BFE, mJ	$AR_{2.5}$
PR	0.463 (±1.57%)	74.4 (±3.44%)	10.4 (±9.51%)
PR70	0.457 (±0.92%)	74.3 (±0.90%)	10.4 (±25.50%)
PR50	0.492 (±1.87%)	83.6 (±9.84%)	13.5 (±21.2%)
PR30	0.499 (±0.95%)	87.9 (±8.59%)	16.2 (±14.80%)
Fresh	0.517 (±0.53%)	102 (±3.48%)	31.2 (±28.80%)

Appendix A. Supplementary Data

[Figure 10 about here.]

[Figure 11 about here.]

[Figure 12 about here.]

[Figure 13 about here.]

List of Figures

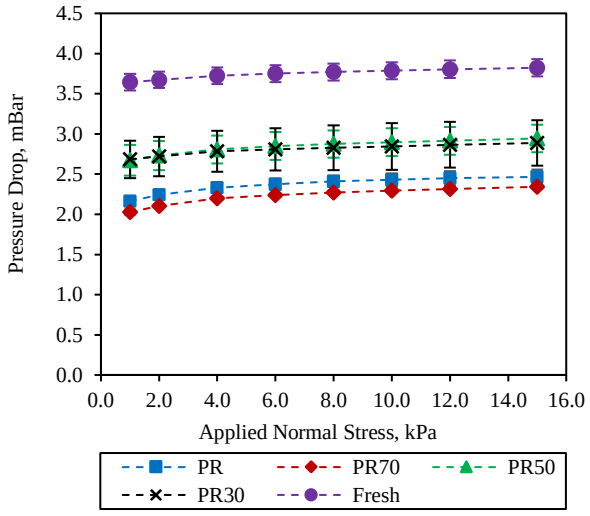

Figure A.1: Pressure drop across five PA12 blends measured at face velocity of 2 mm/s under different consolidation stresses.

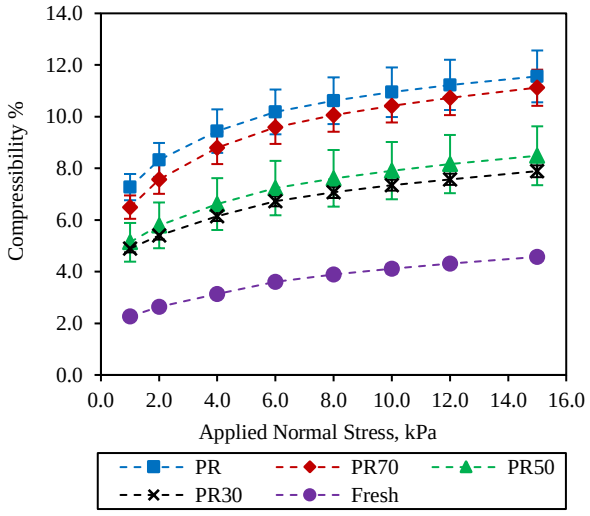

Figure A.2: Compressibility of five blends of PA12 measured at different consolidation stresses.

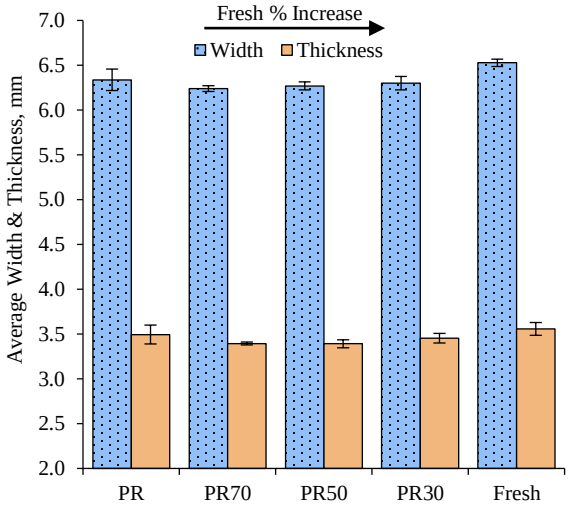

Figure A.3: Average width and thickness of the tensile specimens fabricated from five blends of PA12.

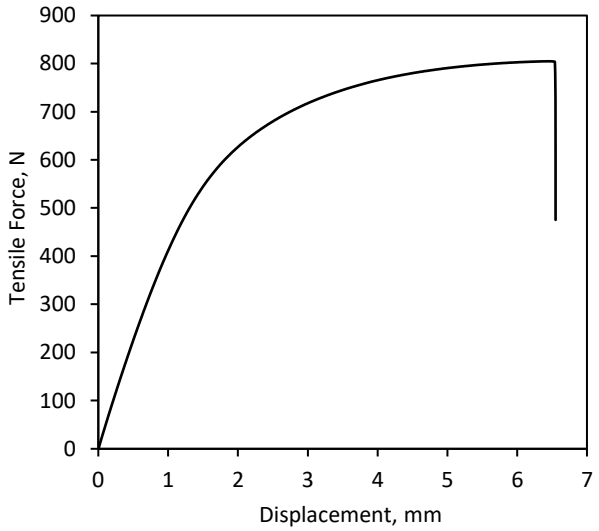

Figure A.4: Force-displacement curve obtained from tensile testing of a Blend C specimen.